A window on exoplanet dynamical histories: Rossiter–McLaughlin observations of WASP-13b and WASP-32b

R. D. Brothwell,[1]⋆ C. A. Watson,[1] G. Hébrard,[2,3] A. H. M. J. Triaud,[4,5] H. M. Cegla,[1]
A. Santerne,[6] E. Hébrard,[7] D. R. Anderson,[8] D. Pollacco,[9] E. K. Simpson,[1]
F. Bouchy,[2,3] D. J. A. Brown,[9] Y. Gómez Maqueo Chew,[9] A. Collier Cameron,[10]
D. J. Armstrong,[9] S. C. C. Barros,[11] J. Bento,[9,12] J. Bochinski,[13] V. Burwitz,[14]
R. Busuttil,[13] L. Delrez,[15] A. P. Doyle,[8] F. Faedi,[9] A. Fumel,[15] M. Gillon,[15]
C. A. Haswell,[13] C. Hellier,[8] E. Jehin,[15] U. Kolb,[13] M. Lendl,[4] C. Liebig,[10]
P. F. L. Maxted,[8] J. McCormac,[9,16] G. R. M. Miller,[10] A. J. Norton,[13] F. Pepe,[4]
D. Queloz,[17] J. Rodríguez,[18] D. Ségransan,[4] I. Skillen,[16] B. Smalley,[8]
K. G. Stassun,[19,20] S. Udry,[4] R. G. West[9] and P. J. Wheatley[9]

Affiliations are listed at the end of the paper

ABSTRACT

We present Rossiter–McLaughlin observations of WASP-13b and WASP-32b and determine the sky-projected angle between the normal of the planetary orbit and the stellar rotation axis (λ). WASP-13b and WASP-32b both have prograde orbits and are consistent with alignment with measured sky-projected angles of $\lambda = 8^{\circ+13}_{-12}$ and $\lambda = -2^{\circ+17}_{-19}$, respectively. Both WASP-13 and WASP-32 have $T_{\rm eff} < 6250$ K, and therefore, these systems support the general trend that aligned planetary systems are preferentially found orbiting cool host stars. A Lomb–Scargle periodogram analysis was carried out on archival SuperWASP data for both systems. A statistically significant stellar rotation period detection (above 99.9 per cent confidence) was identified for the WASP-32 system with $P_{\rm rot} = 11.6 \pm 1.0$ days. This rotation period is in agreement with the predicted stellar rotation period calculated from the stellar radius, R_*, and $v\sin i$ if a stellar inclination of $i_* = 90^{\circ}$ is assumed. With the determined rotation period, the true 3D angle between the stellar rotation axis and the planetary orbit, ψ, was found to be $\psi = 11^{\circ} \pm 14^{\circ}$. We conclude with a discussion on the alignment of systems around cool host stars with $T_{\rm eff} < 6150$ K by calculating the tidal dissipation time-scale. We find that systems with short tidal dissipation time-scales are preferentially aligned and systems with long tidal dissipation time-scales have a broad range of obliquities.

Key words: techniques: photometric – techniques: radial velocities – stars: individual: WASP-13 – stars: individual: WASP-32 – planetary systems.

1 INTRODUCTION

The study of gas giants orbiting close to their host stars allows an insight into the formation and evolution of exoplanets. For example, combined planetary transit photometry and radial velocity (RV) measurements enables the planetary density to be found, providing constraints on the planetary composition. Whilst this provides clues to the formation processes at work, the Rossiter–McLaughlin (RM) effect is thought to be a complementary probe of exoplanet dynamical histories. The RM effect is measured using in-transit spectroscopic observations, revealing a deviation from the Keplerian orbital motion as the star orbits the barycentre of the star–planet system. The effect is caused by the planet occulting the rotating stellar surface. This introduces an asymmetry in the stellar absorption profile, resulting in an apparent shift of the spectral lines. The RM waveform allows the sky-projected spin–orbit alignment angle (λ) between the rotation axis of the host star and the normal to the planetary orbital plane to be determined.

⋆E-mail: rbrothwell01@qub.ac.uk

The alignment angle is thought to provide a window on the dynamical evolution of exoplanets. Hot-Jupiters are thought to form beyond the snow-line where icy cores become massive enough to accrete a gaseous envelope before subsequently migrating either via planet–disc, planet–planet or planet–star interactions. Planet–disc interactions are thought to be dynamically gentle (Goldreich & Tremaine 1980; Lin, Bodenheimer & Richardson 1996) and do not perturb the original inclination of the planet. Other migration mechanisms such as planet–planet and planet–star interactions via the Kozai–Lidov mechanism are more dynamically violent (Kozai 1962; Lidov 1962). The presence of a third body in the system excites periodic oscillations in the eccentricity and inclination of the orbit, where tidal dissipation and circularisation shrinks the semi-major axis. The oscillating inclination resulting from Kozai–Lidov interactions produces a continuum of inclinations with stable orbits. Thus, it is expected that hot-Jupiters will exhibit misaligned orbits if such migration processes are operating.

However, it should be noted that measuring a spin–orbit alignment angle of $\lambda = 0°$ does not necessarily indicate an aligned planetary system. When the impact parameter is low, the RM waveform is independent of λ and instead controls the amplitude, leading to a strong degeneracy between $v \sin i$ and λ (Gaudi & Winn 2007). For example, in a system with an impact parameter of $b = 0$ and/or where the stellar rotation axis is inclined in the direction of the observer, any orientation of the planetary orbit leads to a symmetric RM waveform. By calculating the inclination of the stellar rotation axis, these degeneracies can be broken and the true '3D' system geometry ascertained.

Currently, 76[1] planets have a measured λ where 45 per cent of planets show substantial misalignments. This population of misaligned planets appears to be synonymous with hotter host stars ($T_{\rm eff} \geq 6250$ K) whilst aligned planets are preferentially observed orbiting cool host stars. One proposed reason for the alignment–misalignment transition is a change in the internal structure of main-sequence host stars around 6250 K, where the outer convective envelope is responsible for tidal interactions. Another correlation in current RM data is the degree of alignment with system age (Triaud 2011). All systems with $M_* \geq 1.2\,{\rm M}_\odot$ were considered and systems with ages greater than 2.5 Gyr are preferentially aligned, whereas those below this age are preferentially misaligned. This reflects the development of the convective envelope with system age and lends further support to alignment arising from tidal interactions. Albrecht et al. (2012) showed that other correlations of alignment with the orbital period, ratio of planet mass to stellar mass and possibly orbital distance with λ provide further evidence that realignment is driven by tidal interactions.

In order to interpret the results of RM observations as a tracer of dynamical evolution alone, it must be assumed that the original protoplanetary disc and the star are well aligned. While this seems valid based on angular momentum conservation, theoretical models have begun to challenge this assumption, showing that star–disc misalignment is possible in the pre-main-sequence phase (Bate, Lodato & Pringle 2010; Lai, Foucart & Lin 2011). Thus, measuring λ may not trace planet migration mechanisms but perhaps traces star formation processes or a combination of both. Watson et al. (2011) studied the inclination of resolved debris discs and the inclination of their host stars for nine systems, showing that all are consistent with alignment. The authors note that all systems have

$T_{\rm eff} < 6250$ K and other candidates with $T_{\rm eff} > 6250$ K would be important in exploring the full alignment–misalignment theoretical picture proposed by Winn et al. (2010). Further systems, with a range of spectral types, were investigated by Greaves et al. (2014) where the stellar inclination was found to be aligned with the spatially resolved debris disc for all systems. Recently, Kennedy et al. (2013) tested the alignment of the full star–disc–planet system for HD 82943, the first time the full alignment of a system has been investigated. The complete system (the inclination of the stellar rotation axis, the normal to the disc plane and the normal to the planetary orbit) was found to be aligned at a level similar to the Solar system.

Another approach to distinguish between primordial star–disc misalignments and misalignment driven by migration is to consider the growing number of multiplanet systems. Albrecht et al. (2013) recently analysed the multiple-transiting systems KOI-94 (Hirano et al. 2012) and Kepler-25, finding $\lambda = -11° \pm 11°$ and $\lambda = 7° \pm 8°$, results consistent with alignment. Whilst this was thought to hint that multiplanet systems migrate via planet–disc interactions and hot-Jupiters migrate by a different pathway, evidence for misaligned multiplanet systems has been found (Huber et al. 2013; Walkowicz & Basri 2013). It is clear that a full picture of hot-Jupiter formation and migration is far from complete, requiring the continual building of statistics, preferably beyond the $T_{\rm eff}$ dependence, to explore unstudied regions of parameter space.

In this paper, we report RM observations of WASP-13 and WASP-32. WASP-13 and WASP-32 are both slow rotators (Skillen et al. 2009; Maxted et al. 2010) and cool stars with effective temperatures ~6000 K. Section 2 outlines the observations and analysis procedure. In Section 3, the derived parameters are presented and discussed. Next a search for the stellar rotation period for both systems was investigated. For WASP-32, where a period was found, we then computed the true 3D alignment angle. Finally, we conclude with a discussion of our results in Section 4.

2 DATA ANALYSIS

2.1 Observations and data reduction

All in-transit RV data for WASP-13 and WASP-32 were obtained using the SOPHIE spectrograph mounted on the 1.93 m telescope at the Observatoire de Haute-Provence (OHP). SOPHIE is an environmentally stabilized echelle spectrograph (wavelength range 382–693 nm) designed for high-precision RV measurements. Two 3 arcsec optical fibres were used, with one centred on the target and the other used to simultaneously monitor the sky background in the case of lunar light contamination. The spectra were then reduced using the SOPHIE data reduction pipeline (Perruchot et al. 2008). RVs were extracted using a weighted cross-correlation of each spectrum with a G2 spectral-type mask. A Gaussian was then fitted to the resulting cross-correlation functions to obtain the RV shift. Uncertainties were computed using the empirical relation of Bouchy et al. (2009) and Cameron et al. (2007). The observation and data reduction details particular to each system are presented in Section 3.

2.2 Determination of the system parameters

The RM effect and orbit were fitted simultaneously using all the available spectroscopic data, including previously published orbital data. A Keplerian model was used for the orbit, and the

---

[1] Holt–Rossiter–McLaughlin Encyclopaedia: http://www.physics.mcmaster .ca/~rheller/.

analytical approach described in Ohta, Taruya & Suto (2005, hereafter OTS) was used to model the RM effect. An independent systemic velocity was fitted to each orbital data set in order to account for any instrumental offsets. Similarly, the transit data sets were fitted with separate systemic velocities to incorporate instrumental and long-term stellar activity variations.

To fit the RM effect, the OTS equations were modified to make them dependent on R_p/R_* and a/R_* rather than on R_p, R_* and a, to reflect the parameters derived from photometry, and reduce the number of free parameters. The model comprises 11 parameters: the orbital period, P; mid-transit time, T_0; planetary-to-stellar radius ratio, R_p/R_*; scaled semimajor axis, a/R_*; orbital inclination, i; orbital eccentricity, e; longitude of periastron, ω; RV semi-amplitude of the host star, K; sky-projected angle between the stellar rotation axis and orbital angular momentum vector, λ; projected stellar rotational velocity, $v\sin i$ and the stellar linear limb-darkening coefficient, u.

In summary, the OTS model assumes that the star and transiting planet are discs where the planet is an opaque occulting disc. The RV of a small element on the stellar disc is given by multiplying the x-position of the element (fig. 3 of OTS) by $v\sin i$. This quantity is then weighted by the intensity of the stellar disc at that location and then all the elements are integrated over the entire stellar surface. The OTS equations (see sections 5.1 and 5.2 of OTS) result from assuming a linear limb-darkening law for the stellar intensity. A linear limb-darkening law is assumed as the quadratic model is known to deviate by only a few m s^{-1} from the linear limb-darkening model. Also, it has been shown that by setting u as a free parameter, λ and $v\sin i$ are not significantly affected (Simpson et al. 2011).

A series of parameters included in the model have been derived previously from transit observations (P, R_p/R_*, a/R_* and i_p). These constraints can be included in the fit in the form of a χ^2 penalty function:

$$\chi^2 = \sum_i \left[\frac{v_{i,\text{obs}} - v_{i,\text{calc}}}{\sigma_i} \right]^2 + \left(\frac{X - X_{\text{obs}} + [\sigma_{X_{\text{obs}}} \times G(0,1)]}{\sigma_{X_{\text{obs}}}} \right)^2 ,$$
(1)

where $v_{i,\text{obs}}$ and $v_{i,\text{calc}}$ are the ith observed and calculated RVs from the model, respectively, and σ_i is the corresponding observational error. X is one of the fitted parameters and X_{obs} is the fitted parameter determined from other observations where $\sigma_{X_{\text{obs}}}$ is the associated error. The multiplicative factor $G(0,1)$ is a Gaussian randomly generated number with a mean of 0 and a standard deviation of 1. This includes in the fit the error determined from prior observations. Equation (1) was extended to include all constraints on all parameters where prior parameter information is known. The procedure is described on a case by case basis for each object in the following sections.

To find the best-fitting solution a chi-squared minimization was carried out using the IDL function MPFIT, utilizing the Levenburg–Marquart algorithm. The 1σ best-fitting parameter uncertainties were calculated using a Monte Carlo method. 10^5 synthetic data sets were created by adding a 1σ Gaussian random variable multiplied by the error on the RV to the RV data points. The free parameters were re-optimized for each simulated data set to obtain the distribution of the best-fitting parameter values. The distributions were not assumed to be Gaussian and the 1σ limits were found where the distribution enclosed ±34.1 per cent of the values away from the median. As a consistency check, the data were also analysed using the RML fitting procedure used by, for example, Hébrard et al. (2011a) and Moutou (2011).

3 ANALYSIS

3.1 WASP-13

WASP-13b is a sub-Jupiter mass exoplanet with $M_p = 0.500 \pm 0.037 M_J$ and $R_p = 1.407 \pm 0.052 R_J$ with an orbital period of 4.4 d (Gómez Maqueo Chew et al. 2013). Its host star is a G1V type with $T_{\text{eff}} = 5989 \pm 48$ K, $M_* = 1.187 \pm 0.065$ M$_\odot$, $\log g = 4.16$ and solar metallicity. The host star has a projected rotational velocity of $v\sin i = 5.74 \pm 0.38$ km s^{-1} (Gómez Maqueo Chew et al. 2013).

A transit of WASP-13b was observed with the SOPHIE spectrograph at the 1.93-m telescope at the OHP on the night of 2012 March 6. We acquired a total of 54 spectra, 32 spectra in-transit and 22 spectra out-of-transit with a total of 228 min of out-of-transit data (primarily post-transit). SOPHIE was used in high-efficiency mode (HE) with a resolution of $R = 40\,000$ and fast read-out mode, maintaining a constant signal to noise throughout the observing run (S/N = 30). Typical exposure times were 600 s and the seeing remained ∼2 arcsec during the observing night. The measured RVs are listed in Table 1. Moon illumination was 97 per cent and at a distance of ∼ 30° from WASP-13 on the night of observation. We note that the lunar RV was 0.002 km s^{-1} which, when compared to the systemic velocity of WASP-13 of $\gamma_{\text{orbit}} = 9.8345 \pm 0.0031$ km s^{-1}, means most of the lunar contribution lies outside the stellar absorption-line profile. Nevertheless, we have applied the standard lunar contamination correction available through the SOPHIE data reduction pipeline. To fit the orbit, we used 11 SOPHIE observations acquired during the discovery of the planet (Skillen et al. 2009). The fitted orbit can be found in the left-hand panel of Fig. 1 with the fitted systemic velocity $\gamma_{\text{orbit}} = 9.8345 \pm 0.0031$ km s^{-1} removed from the RV data points.

To fit the RM effect the OTS model was used as described in Section 2.2. The fitted RM waveform can be found in the right-hand panel of Fig. 1 with the systemic velocity $\gamma_{\text{transit}} = 9.7854 \pm 0.0037$ km s^{-1} removed from the RV data points. In the model, the linear limb-darkening coefficient was chosen from the tables of Claret (2004, ATLAS models) for the g' filter. A linear interpolation using John Southworth's JKTLD code with stellar parameters of $T_{\text{eff}} = 5989$ K, $[M/H] = 0.06$, $\log g = 4.16$, $v_{\text{mic}} = 1.27$ km s^{-1} was used and a linear limb-darkening coefficient of $u = 0.75$ was adopted. The eccentricity was fixed at $e = 0$ and a constraint on $v\sin i = 5.74 \pm 0.38$ km s^{-1} was added to the χ^2 penalty function (Gómez Maqueo Chew et al. 2013).

A χ^2 statistic was adopted of the form of equation (1) where the priors included in the penalty function are listed in Table 2. The fitted parameters and uncertainties are given in Table 3. The best-fitting model is shown in Fig. 1 where $\lambda = 8°^{+13}_{-12}$. It is clear from the shape of Fig. 1 that the planet has a prograde orbit. In addition, the RV waveform shows a symmetric shape indicating star–planet alignment. A fit was also attempted with no prior on $v\sin i$ with no effect on the fitted parameters. This is explained by the large impact parameter ($b = 0.6$) where the degeneracy between λ and $v\sin i$ only becomes important in the low-impact parameter regime. In this regime, the form of the RM signal is not strongly dependent on λ; however, the amplitude is controlled by both λ and $v\sin i$. It has been shown that applying a penalty function in this regime has no overall impact on the fitted parameters (Simpson et al. 2011) and this is indeed what we found in the case of WASP-13.

Table 1. RVs and 1σ error bars of WASP-13 measured with SOPHIE during and outside transit.

BJD −240 0000	RV (km s^{-1})	Error (km s^{-1})
5993.314 09	9.7904	0.0145
5993.321 50	9.8080	0.0146
5993.329 02	9.8182	0.0155
5993.336 02	9.8084	0.0141
5993.342 63	9.8009	0.0140
5993.348 59	9.8145	0.0137
5993.354 43	9.8019	0.0140
5993.360 88	9.8099	0.0139
5993.369 32	9.7990	0.0143
5993.375 64	9.7856	0.0134
5993.380 98	9.7665	0.0135
5993.386 34	9.7953	0.0134
5993.391 86	9.8092	0.0135
5993.397 93	9.7967	0.0135
5993.405 06	9.7772	0.0137
5993.411 12	9.7625	0.0137
5993.417 08	9.7577	0.0135
5993.423 17	9.7603	0.0136
5993.429 85	9.7796	0.0140
5993.436 24	9.7763	0.0137
5993.442 25	9.7706	0.0137
5993.447 45	9.7376	0.0136
5993.452 16	9.7776	0.0133
5993.456 49	9.7616	0.0132
5993.460 69	9.7642	0.0131
5993.464 83	9.7555	0.0130
5993.473 32	9.7646	0.0128
5993.477 73	9.7833	0.0128
5993.482 56	9.7792	0.0132
5993.488 52	9.7982	0.0139
5993.495 31	9.7980	0.0141
5993.501 70	9.7743	0.0136
5993.508 20	9.7951	0.0136
5993.514 31	9.7916	0.0135
5993.520 41	9.7521	0.0134
5993.526 15	9.7550	0.0133
5993.531 77	9.7796	0.0133
5993.537 39	9.7534	0.0132
5993.543 92	9.7606	0.0134
5993.549 66	9.7866	0.0137
5993.555 66	9.7685	0.0136
5993.561 68	9.7801	0.0134
5993.567 63	9.7688	0.0137
5993.574 12	9.7764	0.0140
5993.581 27	9.7691	0.0137
5993.588 13	9.7442	0.0139
5993.594 83	9.7579	0.0137
5993.601 64	9.7778	0.0143
5993.608 65	9.7475	0.0140
5993.614 94	9.7584	0.0137
5993.621 45	9.7903	0.0142
5993.628 27	9.7537	0.0153
5993.635 58	9.7447	0.0148
5993.642 69	9.7797	0.0145

3.2 WASP-32

WASP-32 is a massive exoplanet with $M_p = 3.60 \pm 0.07 M_J$ and $R_p = 1.19 \pm 0.06 R_J$ in a $P = 2.7$ d orbit. The host star has $T_{eff} = 6100 \pm 100$ K, $M_* = 1.10 \pm 0.03$ M$_\odot$, $\log g = 4.4$ and is lithium depleted (Maxted et al. 2010). The projected rotational velocity of the host star is $v \sin i = 4.8 \pm 0.8$ km s^{-1} (Maxted et al. 2010).

We acquired 22 spectra during the transit of WASP-32, covering the complete transit. Four spectra were acquired prior to transit and eight spectra were acquired post transit with a total of 168 min of observations acquired outside transit. The data were obtained using SOPHIE on the night of 2011 August 29, with clear conditions and a typical seeing of 2.5 arcsec. SOPHIE was operated in HE mode and there was no moonlight pollution on the night of observation. The derived RVs can be found in Table 4. To fit the orbit, 14 CORALIE out-of-transit RVs were used from the WASP-32 discovery paper (Maxted et al. 2010). The fitted orbit can be found in the left-hand panel of Fig. 2 with the systemic velocity offset $\gamma_{orbit} = 18.2796^{+0.0061}_{-0.0062}$ km s^{-1} removed from the RV data points.

To fit the RM effect, the OTS model was used as described in Section 2.2. The fitted RM waveform can be found in the right-hand panel of Fig. 2 with the systemic velocity $\gamma_{transit} = 18.1698 \pm 0.0095$ km s^{-1} removed from the RV data points. We note that the difference in the orbital and transit systemic velocities is ∼100 m s^{-1} for WASP-32 and ∼50 m s^{-1} for WASP-13, comparable to values obtained for other objects in the literature. In particular, Simpson et al. (2010) measured a difference in the orbital and transit velocities for WASP-1b of ∼200 m s^{-1} using the same RM model and observational approach. Also we examined the likelihood that the measured systemic velocity offsets could be driven by long-term stellar activity by phase-folding the WASP-13 and WASP-32 light curves with the transits removed. A clear sinusoidal photometric modulation was detected in the light curve for WASP-32 at the ∼2 per cent level, although modulations were not detected for WASP-13. The increased activity level of WASP-32 also explains why a period peak was detected in the periodogram (discussed in Section 3.3). Using the relation presented in Saar & Donahue (1997) the RV shift due to inhomogeneous spot coverage can be estimated. An ∼100 m s^{-1} RV shift for WASP-32 is expected with ∼2 per cent inhomogeneous spot coverage, comparable to the difference in our reported systemic velocity for WASP-32 compared to the systemic velocity of the orbital data. Therefore, the difference in systemic velocities may be explained by spot coverage. It is important to note that the RM effect duration for WASP-32 is ∼2.4 h, during which the host star rotates by ∼8°. Thus, it is unlikely that new spot features would rotate into view during transit, and thus, systemic velocity offsets over the course of the RM observation are insignificant.

In the model the linear limb-darkening coefficient was chosen as before with stellar parameters of $T_{eff} = 6100$ K, $[M/H] = -0.13$, $\log g = 4.39$, $v_{mic} = 2$ km s^{-1}, resulting in a linear limb-darkening coefficient of $u = 0.71$. WASP-32 is a reasonably eccentric system with $e = 0.018 \pm 0.0065$ and this parameter was fixed in the RM fit.

A χ^2 statistic was adopted of the form of equation (1), where the priors included in the penalty function are taken from Maxted et al. (2010) and are listed in Table 2. The best-fitting model is shown in Fig. 2 where $\lambda = -2^{\circ+17}_{-19}$ and the fitted parameters are listed in Table 5. It is clear from Fig. 2 that WASP-32 has a symmetric RM waveform, moving from redshift to blueshift, consistent with an aligned prograde orbit. The fitted λ is
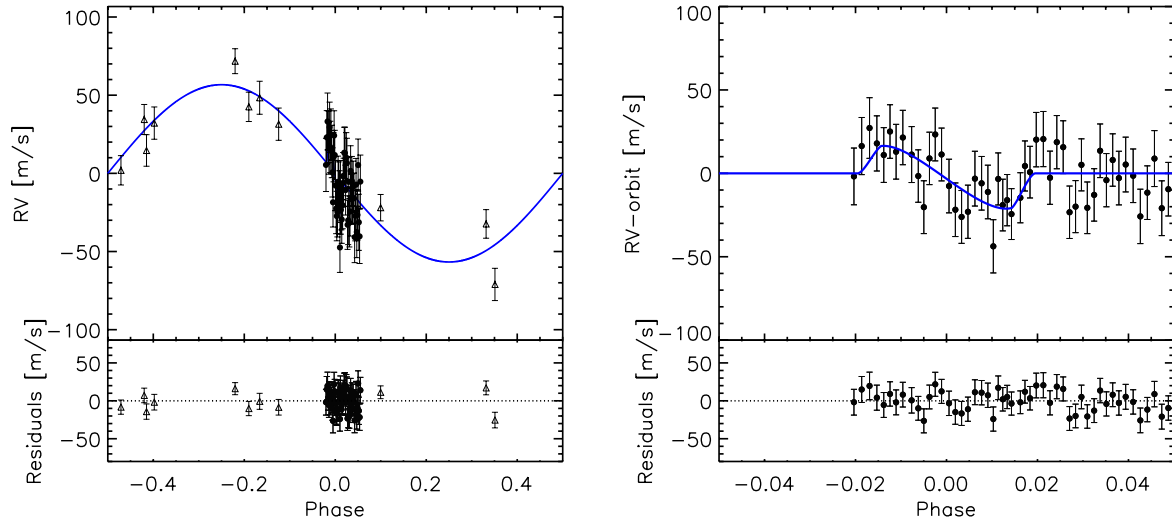
Figure 1. *Left-hand panel*: WASP-13 phase-folded orbit minus the systemic velocity overplotted with the best-fitting model (solid line). Out-of-transit RVs of Skillen et al. (2009) are displayed as open triangles and the measured RVs using SOPHIE at the OHP on the night 2012 March 6 are displayed as filled circles. *Right-hand panel*: spectroscopic transit minus the orbital velocity, overplotted with the best-fitting RM model with the residuals shown below.

Table 2. Adopted system parameters and uncertainties used to model the RM effect, and other photometric parameters used in this work. The reference is indicated at the end of the column for each object.

Parameter (units)	Symbol	WASP-13	WASP-32
Orbital period (d)	P	4.3530135 ± 0.0000027	2.718659 ± 0.000008
Transit epoch	T_0	$2455305.62823 \pm 0.00025(\mathrm{BJD_{UTC}})$	$2455151.0546 \pm 0.0005(\mathrm{HJD})$
Transit duration (h)	T_d	4.003 ± 0.024	2.424 ± 0.048
Orbital inclination (°)	i	85.43 ± 0.29	85.3 ± 0.5
Planet/star radius ratio	R_p/R_*	0.0919 ± 0.0126	0.11 ± 0.01
Scaled semimajor axis	a/R_*	7.54 ± 0.27	7.63 ± 0.35
Eccentricity	e	0 (adopted)	0.0180 ± 0.0065
Reference		Gómez Maqueo Chew et al. (2013)	Maxted et al. (2010)

Table 3. Derived system parameters and uncertainties for WASP-13. The effective temperature is taken from Gómez Maqueo Chew et al. (2013). Fitted free parameters are listed with the corresponding errors followed by the parameters controlled by priors (listed in Table 2).

Parameter (units)	Symbol	Value
Free parameters:		
Projected alignment angle (°)	λ	8^{+13}_{-12}
Projected stellar rotation velocity (km s^{-1})	$v\sin i$	5.7 ± 0.4
RV semi-amplitude (km s^{-1})	K	0.0564 ± 0.0043
Systemic velocity of SOPHIE transit data set (km s^{-1})	$\gamma_{\mathrm{transit}}$	9.7854 ± 0.0037
Systemic velocity of SOPHIE orbital data set (km s^{-1})	γ_{orbit}	9.8345 ± 0.0031
Parameters controlled by priors:		
Period (d)	P	4.3530135 ± 0.000003
Transit epoch (BJD$_{\mathrm{UTC}}$ − 2400000)	T_0	5304.53998 ± 0.00025
Planet/star radius ratio	R_p/R_*	$0.0918^{+0.0127}_{-0.0126}$
Scaled semimajor axis	a/R_*	7.54 ± 0.27
Orbital inclination (°)	i	85.43 ± 0.29
Fixed parameters:		
Eccentricity	e	0
Limb darkening	u	0.75
Effective temperature (K)	T_{eff}	5989 ± 48

Table 4. RVs and 1σ error bars of WASP-32 measured with SOPHIE during and outside transit.

BJD $-240\,0000$	RV (km s^{-1})	Error (km s^{-1})
5803.443 75	18.2586	0.0230
5803.456 34	18.2510	0.0229
5803.468 88	18.2249	0.0231
5803.479 19	18.2285	0.0225
5803.488 88	18.2439	0.0230
5803.499 42	18.2344	0.0231
5803.509 22	18.2643	0.0224
5803.518 74	18.2419	0.0222
5803.529 52	18.2165	0.0228
5803.540 57	18.1203	0.0217
5803.551 90	18.1145	0.0221
5803.563 03	18.0880	0.0225
5803.573 13	18.1301	0.0219
5803.583 78	18.1474	0.0213
5803.594 28	18.0968	0.0216
5803.605 08	18.0819	0.0214
5803.615 74	18.0997	0.0218
5803.626 40	18.0852	0.0220
5803.636 63	18.0709	0.0220
5803.646 35	18.0726	0.0224
5803.655 82	18.0417	0.0222
5803.665 34	18.0676	0.0298

consistent with that found recently by Brown et al. (2012) where $\lambda = 10.5^{\circ\,+6.4}_{\;-5.9}$.

The fitted $v \sin i = 7.6^{+4.2}_{-3.1}$ km s^{-1} is consistent with that found from sprectroscopic fitting, $v\sin i = 4.8 \pm 0.8$ km s^{-1} (Maxted et al. 2010) and the measured $v \sin i = 3.9^{+0.4}_{-0.5}$ km s^{-1} derived from Doppler Tomography (Brown et al. 2012). However, our determined $v\sin i$ is noticeably larger than the others that have been found. Thus, a fit with a prior on $v\sin i$ set to that found by Brown et al. (2012) was attempted. It was found that λ is insensitive to fixing $v\sin i$ in the fit, with little change in $\chi^2_{\rm red}$. Thus, the fit with a prior on $v\sin i$ was taken as our adopted solution with a fitted $\lambda = -2^{\circ\,+17}_{\;-19}$ and $v\sin i = 3.9 \pm 0.5$ km s^{-1}. Also we attempted a fit using the

Brown et al. (2012) HARPS RVs alone and found that the error bars on λ were increased relative to the Brown et al. (2012) results. We attribute this to the use of simultaneous photometry in the Brown et al. (2012) analysis but note our fit is the first independent analysis on the alignment of WASP-32b.

3.3 3D alignment angle

Modelling the RM effect leads to a determination of the sky-projected alignment angle, λ. As a consequence of only measuring the sky-projected alignment angle, in some cases a measured λ that indicates an aligned planet may actually be a misaligned system. For example, measuring a $\lambda = 0^{\circ}$ does not necessarily indicate an aligned planetary system if the inclination of the stellar rotation axis is unknown. If the stellar rotation axis is inclined relative to the line of sight or if the impact parameter, b, is close to 0, then the planet may be misaligned but the symmetry of the RM waveform would indicate an aligned system. A true three-dimensional reconstruction of the system geometry can be gleaned if the inclination of the host star can be found simultaneously with the sky-projected angle, removing any possible ambiguities that remain from RM observations alone.

By determining the stellar rotation period ($P_{\rm rot}$) combined with the projected rotational velocity ($v\sin i$) and stellar radius (R_*), the stellar inclination (i_*) can be found via

$$\sin i_* = P_{\rm rot} \times \left(\frac{v \sin i_*}{2\pi R_*} \right). \tag{2}$$

The projected stellar rotational velocity, $v\sin i$, and stellar radius estimates can be obtained via spectral analysis. There are a number of ways to determine the stellar rotation period, to determine i_*, either by monitoring Ca H&K emission or photometric monitoring of starspots (e.g. Simpson et al. 2010, Watson et al. 2010). In our analysis, we adopt the latter, where the modification of disc integrated light indicates the passage of starspots across the stellar surface. By sourcing the detrended WASP light curves for WASP-13 and WASP-32, an extensive Lomb–Scargle (Lomb 1976; Scargle 1982) periodogram analysis was carried out to search for significant stellar rotation periods. The significance of the periods was estimated
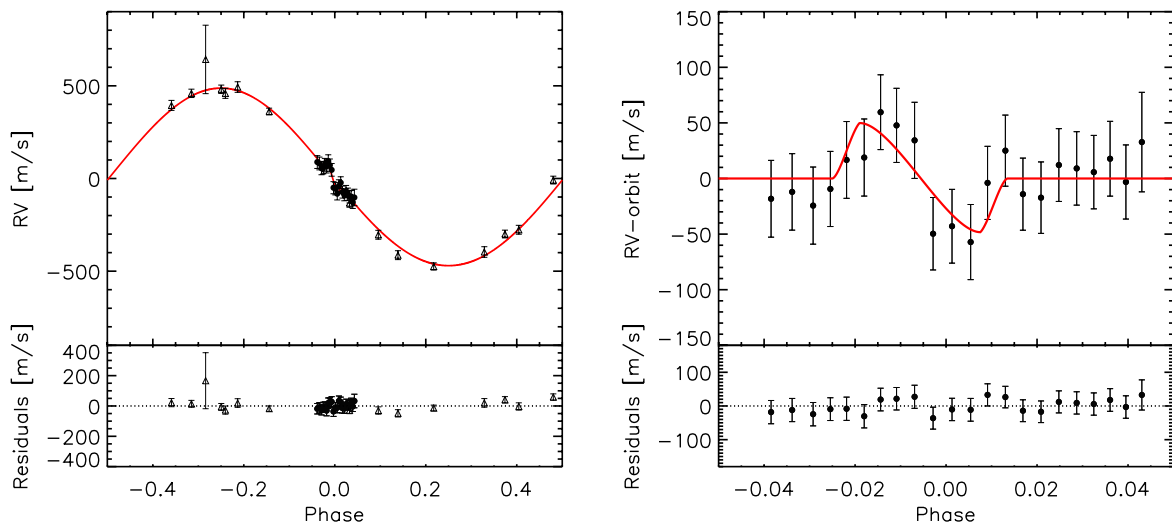
Figure 2. *Left-hand panel*: WASP-32 phase-folded orbit minus the systemic velocity overplotted with the best-fitting model (solid line). Out-of-transit RVs of Maxted et al. (2010) from CORALIE are displayed as open triangles and the measured RVs using SOPHIE are displayed as filled circles. *Right-hand panel*: spectroscopic transit minus the orbital velocity, overplotted with the best-fitting RM model with the residuals shown below.

Table 5. Derived system parameters and uncertainties for WASP-32. The effective temperature is taken from Maxted et al. (2010). The parameters controlled by priors are listed in Table 2.

Parameter (units)	Symbol	Value
Free parameters:		
Projected alignment angle (°)	λ	-2^{+17}_{-19}
RV semi-amplitude (km s^{-1})	K	$0.4789^{+0.0079}_{-0.0078}$
Systemic velocity of SOPHIE transit data set (km s^{-1})	γ_{transit}	18.1698 ± 0.0095
Systemic velocity of SOPHIE orbital data set (km s^{-1})	γ_{orbit}	$18.2796^{+0.0061}_{-0.0062}$
Parameters controlled by priors:		
Projected stellar rotation velocity (km s^{-1})	$v\sin i$	3.9 ± 0.5
Period (d)	P	$2.718\,6590 \pm 0.000\,008$
Transit epoch (HJD $- 240\,0000$)	T_0	$5150.390\,51 \pm 0.000\,50$
Planet/star radius ratio	R_p/R_*	0.1091 ± 0.0010
Scaled semimajor axis	a/R_*	7.63 ± 0.35
Orbital inclination (°)	i	85.30 ± 0.50
Fixed parameters:		
Eccentricity	e	0.018 ± 0.0065
Limb darkening	u	0.71
Effective temperature (K)	T_{eff}	6100 ± 100

using the false alarm probability (FAP; Horne & Baliunas 1986). A detection was defined when the peak in the periodogram surpassed the 0.1 per cent FAP power level. This means the detected period has a 99.9 per cent confidence level that it does not arise by chance. Before carrying out the periodogram analysis on all sourced light curves, the updated transit ephemeris was used to remove the planetary transits. This prevented unwanted harmonics entering the periodograms and ensured intrinsic stellar periodicities were analysed.

As a useful comparison, assuming the rotation axis is perpendicular to the line of sight ($i_* = 90°$), P_{rot} can be computed for all three systems using the $v\sin i$ quoted for all three systems in Section 3. In the case of WASP-32, a number of $v\sin i$ measurements have been determined but we use $v\sin i = 3.9^{+0.4}_{-0.5}$ km s^{-1} from Doppler Tomography (Brown et al. 2012) to compute the stellar inclination for WASP-32. For WASP-13 and WASP-32, true alignment would lead to expected values of the stellar rotation period of $P_{\text{rot}} = 17.1$ and 11.7 d, respectively. No statistically significant rotation period was detected for WASP-13, however a statistically significant period was detected in the WASP-32 data above the 99.9 per cent confidence level. The detected period is $P_{\text{rot}} = 11.6 \pm 1.0$ d and the periodogram is shown in Fig. 3. With P_{rot} known, i_* can be determined from equation (2), where an $i_* = 81° \pm 9°$ was found. This, combined with the planetary inclination (i_p) determined from the planetary transit and λ, allows the true 3D alignment angle, ψ, to be found via

$$\cos\psi = \cos i_* \cos i_p + \sin i_* \sin i_p \cos\lambda. \qquad (3)$$

The measured 3D alignment angle, using $\lambda = 10.5^{°+6.4}_{-5.9}$ from Brown et al. (2012) gives $\psi = 11° \pm 14°$ and using the value of $\lambda = -2^{°+17}_{-19}$, derived in this work, $\psi = 2° \pm 16°$. Both results indicate that the planet is aligned when considered as a 3D system.

4 CONCLUSIONS

The spectroscopic transits of WASP-13b and WASP-32b were observed with the SOPHIE spectrograph and the projected spin–orbit alignment was determined for both systems where $\lambda = 8^{°+13}_{-12}$ and $-2^{°+17}_{-19}$, respectively. WASP-13 and WASP-32 are consistent with alignment within 1σ. This suggests WASP-13 and WASP-32 had a
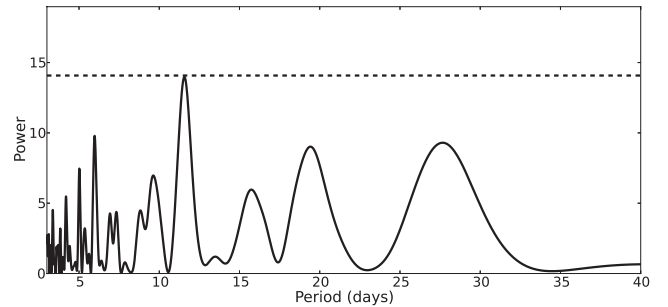
Figure 3. Lomb–Scargle periodogram analysis for the detrended WASP-32 light curve from the SuperWASP data archive, observed in the date range interval 5048.570 567 13 – – 5153.428 136 57 HJD and with planetary transits removed. The dashed line indicates the FAP of 0.1 per cent and indicates the level where a period detection is defined. The peak period corresponds to $P_{\text{rot}} = 11.6 \pm 1.0$ d and is at the 0.1 per cent FAP power level. The peak at 5.8 d is a harmonic of the peak detected period.

gentle migration history and remained unperturbed from the original obliquity of the protoplanetary disc. An alternative scenario is the gradual loss of orbital energy by the planet through tidal dissipation, acting to realign the stellar spin and planetary orbital axes over a long enough time-scale (Winn et al. 2010). The misalignment angle measured for WASP-32 in this work is consistent with the value of $\lambda = 10.5^{+6.4}_{-6.5}$ measured by Brown et al. (2012). Our measured 3D alignment angle of $\psi = 11° \pm 14°$ provides further evidence that the system is well aligned. It is important to note that ψ has not been measured for many systems (see Table 6) and WASP-32 adds to the number of systems with a measured 3D alignment angle. Further, Table 6 shows that some systems are unambiguously aligned. Attempts have been made to derive the original obliquity distribution (Triaud et al. 2010; Li 2013) assuming a $\cos i_*$ probability distribution in the stellar inclination; however, this deprojection technique means that cases where $i_* = 90°$ are unaccounted for. All current measurements of ψ in Table 6 show that there is a bimodal distribution in ψ: a planetary population that is aligned and one that is near isotropic. Thus, any attempt to deproject the population of spin–orbit angles is destined to fail if current trends in i_* are not recognized.

Table 6. All cases where the 3D alignment angle, ψ, has been reported in the literature. The measured ψ and reference is indicated in the table. Multiple references indicate where ψ has been measured in separate studies. Cases where multiple ψ measurements are listed with a single reference stems from orbital geometry degeneracies. Our result for WASP-32 adds to the number of systems with a complete 3D alignment angle determination.

Object	$\psi (°)$	Reference
CoRoT-18b	20 ± 20	[1]
HAT-P-7	>86.1	[2]
HAT-P-11	$106^{+15}_{-11}, 97^{+8}_{-4}$	[3]
Kepler-16(AB)b	<18.3	[4]
Kepler-17b	0 ± 15	[5]
Kepler-63b	104^{+9}_{-14}	[6]
Kepler-13.01	$54 \pm 4, 56 \pm 4, 124 \pm 4, 126 \pm 4$	[7]
KOI-368.01	69^{+9}_{-10}	[8]
PTFO 8-86956b	73.1 ± 0.5	[9]
WASP-15b	>90.3	[10]
WASP-17b	$>91.7, >92.6$	[10], [11]
WASP-19b	$<19, <20$	[10], [12]
WASP-32b	**11 ± 14**	**This Work**

[1] Hébrard et al. (2011b) [2] Winn et al. (2009) [3] Sanchis-Ojeda & Winn (2011) [4] Winn et al. (2011) [5] Désert et al. (2011) [6] Sanchis-Ojeda et al. (2013) [7] Barnes, Linscott & Shporer (2011) [8] Zhou & Huang (2013) [9] Barnes et al. (2013) [10] Triaud et al. (2010) [11] Bayliss et al. (2010) [12] Hellier et al. (2011).

Winn et al. (2010) proposed one mechanism that could explain the observed distribution of alignment angles via tidal dissipation with the host star. In this scheme, aligned planets are expected around cool stars ($T_{eff} < 6250$ K) and misaligned planets are expected orbiting hot host stars ($T_{eff} > 6250$ K). WASP-13 and WASP-32 have $T_{eff} = 5989 \pm 48$ and 6100 ± 100 K, respectively, and therefore both lie in the cool regime. Thus, both WASP-13 and WASP-32 add further evidence to alignment arising from tidal interactions. Also it must be noted that WASP-32 has a T_{eff} close to 6250 K, perhaps indicating that it is possible for massive planets (in this case with a mass $>3M_J$) to tidally realign around relatively hot host stars.

Alignment is expected to be determined by planet–star tidal interactions. The tidal interaction time-scale due to tidal dissipation in the convective envelope is related to q, the planet to star mass ratio, and the scaled semimajor axis, a/R_* (see equation 2 of Albrecht et al. 2013):

$$\frac{1}{\tau_{CE}} = \frac{1}{10 \times 10^9 \text{ yr}} q^2 \left(\frac{a/R_*}{40}\right)^{-6}. \quad (4)$$

Thus, the above equation shows that $\tau_{CE} \propto q^{-2} \times (a/R_*)^6$. As planet–star tidal interactions with the convective envelope are thought to be responsible for aligning hot-Jupiters via tidal damping, we modified equation (4) to include the convective mass of the planet host, M_{conv}. Thus, in Fig. 4, an ensemble of systems with RM measurements are plotted against $(M_p/M_{conv})^{-1/3} \times (a/R_*)$, a quantity proportional to the tidal dissipation time-scale. The convective envelope mass, M_{conv}, was derived using the EZ-WEB stellar evolution code.[2] To run the stellar models, the age of the system is required. For systems lacking derived ages, we have assumed an age of 4 Gyr, but note the results are largely insensitive to age. Note the

[2] EZ-WEB stellar evolution code: http://www.astro.wisc.edu/~townsend/static.php?ref=ez-web.

x-axis scale was chosen such that $\tau_{CE}^{1/6} \propto (M_p/M_{conv})^{-1/3} \times (a/R_*)$ for plotting convenience. As suggested by Zahn (1977) tides are dissipated more effectively when the planet orbits a star with a convective envelope. Winn et al. (2010) have postulated that tides have changed the distribution of spin–orbit angles with $T_{eff} < 6150$ K but left the distribution unaltered with $T_{eff} > 6350$ K. Thus, only 'cool' systems with $T_{eff} < 6150$ K are plotted in Fig. 4. It can be observed that as the tides become weaker (when the tidal dissipation time-scale increases), there is some evidence that misaligned orbits are more likely. WASP-13 and WASP-32 are plotted in Fig. 4 and are consistent with alignment. A recent addition to the ensemble of RM measurements is WASP-80b (Triaud et al. 2013), a K7-M0 star and the coolest host star in the sample with $T_{eff} = 4145 \pm 100$ K. Even as the coolest system, the planet is on an inclined circular orbit with $|\lambda| = 75°$ similar to the spin–orbit angle measured around hotter mid-F stars. This suggests that hot-Jupiters may have been more frequently misaligned in the past. However, other mechanisms could act to misalign a system such as the presence of another perturbing body or if the host star is not old enough to develop a convective envelope. WASP-80b is considered a rare example of a misaligned system around a cool host star (Triaud et al. 2013). However, Fig. 4 suggests that WASP-80b is yet to realign because of its long tidal dissipation time-scale.

Even though the above analysis is simplified, Fig. 4 suggests that planet–star tidal interactions likely play a role in damping the obliquities of hot-Jupiters around cool host stars. Systems with short tidal dissipation time-scales are preferentially aligned; however, those with longer time-scales show an apparent random distribution in λ. This may suggest that hot-Jupiters once had a broader range of obliquities in the past and that they have been realigned over time via tidal interactions (Albrecht et al. 2013). In Fig. 4, WASP-8b is the most obvious outlier in the distribution; however, WASP-8 is a dynamically complex system with suggestions the Kozai mechanism or violent dynamical interactions may explain the misaligned orbit (Queloz et al. 2010).

It is known that stars with $M > 1.2 \, M_\odot$ cool as they evolve along the main sequence. As the star cools an outer convective envelope develops, increasing the strength of the tidal interactions. Thus, the distribution of spin–orbit angles is expected to change with time where a planet originally on a misaligned orbit will realign as the convective envelope of the host star develops. Triaud 2011 plotted $|\lambda|$ against age for all systems with $M > 1.2 \, M_\odot$. The plot provides weak evidence that the spin–orbit alignment distribution changes with time and is another manifestation of the influence of tidal interactions. Objects with ages 2.5–3 Gyr appear aligned, whereas more misaligned systems are observed around stars with younger ages. Even though the plots of $|\lambda|$ against a/R_* and age show evidence for evolution due to tides, it is still unclear if an original misaligned hot-Jupiter population would survive realignment around 'cool' host stars or tidally infall into the star, leaving the aligned population observed today.

We have presented RM measurements for WASP-13 and WASP-32. Analysing out-of-transit survey photometry for WASP-32 revealed the rotation period of the host star, and thus, the 3D alignment angle $\psi = 11° \pm 14°$ of the planetary system. WASP-32 adds to the number of systems with a full 3D alignment angle determination. It is clear that it is becoming increasingly important to investigate the full star–planet–disc (e.g. Watson et al. 2011; Kennedy et al. 2013) alignment in order to fully assess the migration history of exoplanets. Only with an alignment determination of the whole system can we begin to fully evaluate the migration scenarios of hot-Jupiters.
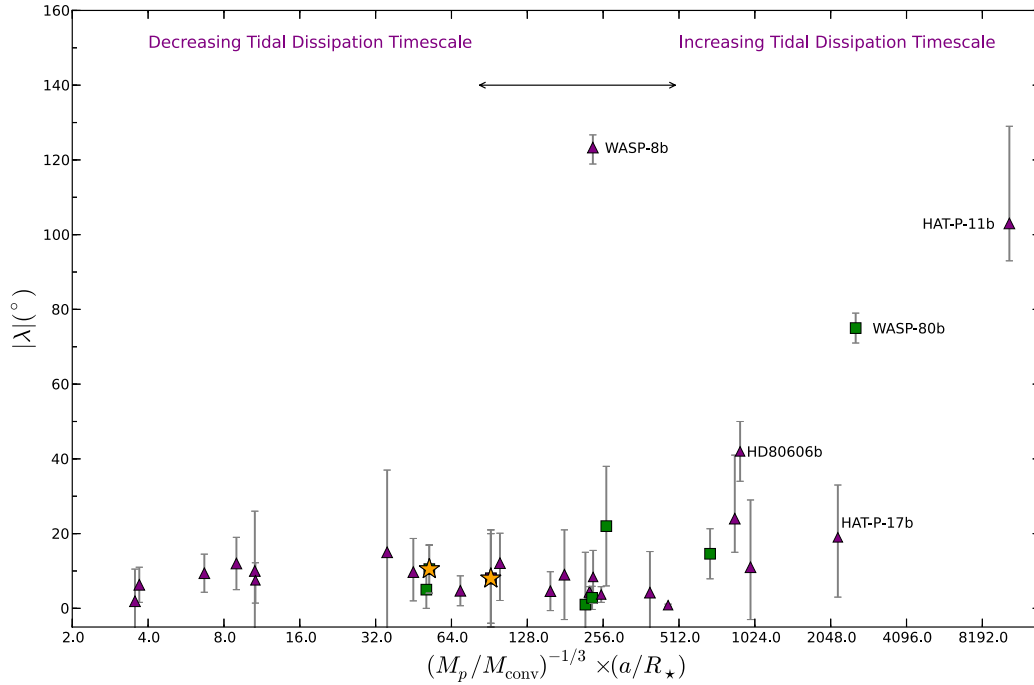
Figure 4. Plot of $|\lambda|$ against $(M_{\mathrm{p}}/M_{\mathrm{conv}})^{-1/3} \times (a/R_*)$ for all systems with $T_{\mathrm{eff}} < 6150$ K. a/R_* is obtained directly from the planetary transit. The convective mass, M_{conv}, was derived from the EZ-WEB stellar evolution code. Systems with age determinations are shown as triangle symbols and those with an assumed age of 4 Gyr are shown as square symbols. WASP-13b and WASP-32b are shown as starred symbols on the plot.

REFERENCES

Albrecht S. et al., 2012, ApJ, 757, 18
Albrecht S., Winn J. N., Marcy G. W., Howard A. W., Isaacson H., Johnson J. A., 2013, ApJ, 771, 11
Barnes J. W., Linscott E., Shporer A., 2011, ApJS, 197, 10
Barnes J. W., van Eyken J. C., Jackson B. K., Ciardi D. R., Fortney J. J., 2013, ApJ, 774, 53
Bate M. R., Lodato G., Pringle J. E., 2010, MNRAS, 401, 1505
Bayliss D. D. R., Winn J. N., Mardling R. A., Sackett P. D., 2010, ApJ, 722, L224
Bouchy F. et al., 2009, A&A, 505, 853
Brown D. J. A. et al., 2012, ApJ, 760, 139
Cameron A. C. et al., 2007, MNRAS, 375, 951
Claret A., 2004, A&A, 428, 1001
Désert J.-M. et al., 2011, ApJS, 197, 14
Gaudi B. S., Winn J. N., 2007, ApJ, 655, 550
Goldreich P., Tremaine S., 1980, ApJ, 241, 425
Gómez Maqueo Chew Y. et al., 2013, ApJ, 768, 79
Greaves J. S. et al., 2014, MNRAS, 438, L31
Hébrard G. et al., 2011a, A&A, 527, L11
Hébrard G. et al., 2011b, A&A, 533, A130
Hellier C., Anderson D. R., Collier-Cameron A., Miller G. R. M., Queloz D., Smalley B., Southworth J., Triaud A. H. M. J., 2011, ApJ, 730, L31
Hirano T. et al., 2012, ApJ, 759, L36
Horne J. H., Baliunas S. L., 1986, ApJ, 302, 757
Huber D. et al., 2013, Science, 342, 331
Kennedy G. M., Wyatt M. C., Bryden G., Wittenmyer R., Sibthorpe B., 2013, MNRAS, 436, 898
Kozai Y., 1962, ApJ, 67, 591
Lai D., Foucart F., Lin D. N. C., 2011, MNRAS, 412, 2790
Li G., Naoz S., Kocsis B., Loeb A., 2013, preprint (arXiv:1310.6044)
Lidov M. L., 1962, Planet. Space Sci., 9, 719
Lin D. N. C., Bodenheimer P., Richardson D. C., 1996, Nature, 380, 606
Lomb N. R., 1976, Ap&SS, 39, 447
Maxted P. F. L. et al., 2010, PASP, 122, 1465
Moutou C. et al., 2011, A&A, 533, A113
Ohta Y., Taruya A., Suto Y., 2005, ApJ, 622, 1118 (OTS)
Perruchot S. et al., 2008, Proc. SPIE, 7014E, 70140J
Queloz D. et al., 2010, A&A, 517, L1
Saar S. H., Donahue R. A., 1997, ApJ, 485, 319
Sanchis-Ojeda R., Winn J. N., 2011, ApJ, 743, 61
Sanchis-Ojeda R. et al., 2013, ApJ, 775, 54

Scargle J. D., 1982, ApJ, 263, 835

Simpson E. K., Baliunas S. L., Henry G. W., Watson C. A., 2010, MNRAS, 408, 1666

Simpson E. K. et al., 2011, MNRAS, 414, 3023

Skillen I. et al., 2009, A&A, 502, 391

Triaud A. H. M. J., 2011, A&A, 534, L6

Triaud A. H. M. J. et al., 2010, A&A, 524, A25

Triaud A. H. M. J. et al., 2013, A&A, 551, A80

Walkowicz L. M., Basri G. S., 2013, MNRAS, 436, 1883

Watson C. A., Littlefair S. P., Collier Cameron A., Dhillon V. S., Simpson E. K., 2010, MNRAS, 408, 1606

Watson C. A., Littlefair S. P., Diamond C., Collier Cameron A., Fitzsimmons A., Simpson E., Moulds V., Pollacco D., 2011, MNRAS, 413, L71

Winn J. N., Johnson J. A., Albrecht S., Howard A. W., Marcy G. W., Crossfield I. J., Holman M. J., 2009, ApJ, 703, L99

Winn J. N., Fabrycky D., Albrecht S., Johnson J. A., 2010, ApJ, 718, L145

Winn J. N. et al., 2011, ApJ, 741, L1

Zahn J.-P., 1977, A&A, 57, 383

Zhou G., Huang C. X., 2013, ApJ, 776, L35

[1]*Astrophysics Research Centre, School of Mathematics & Physics, Queen's University, Belfast BT7 1NN, UK*

[2]*Institut d'Astrophysique de Paris, UMR7095 CNRS, Université Pierre & Marie Curie, 98bis boulevard Arago, F-75014 Paris, France*

[3]*Observatoire de Haute-Provence, CNRS/OAMP, F-04870 St Michel l'Observatoire, France*

[4]*Observatoire astronomique de l'Université de Genève, 51 ch. des Maillettes, CH-1290 Sauverny, Switzerland*

[5]*Department of Physics, and Kavli Institute for Astrophysics and Space Research, Massachusetts Institute of Technology, Cambridge, MA 02139, USA*

[6]*Centro de Astrofísica, Universidade do Porto, Rua das Estrellas, P-4150-762 Porto, Portugal*

[7]*IRAP-UMR 5277, CNRS and Univ. de Toulouse, 14 Av. E. Belin, F-31400 Toulouse, France*

[8]*Astrophysics Group, Keele University, Staffordshire ST5 5BG, UK*

[9]*Department of Physics, University of Warwick, Coventry CV4 7AL, UK*

[10]*School of Physics and Astronomy, University of St Andrews, North Haugh, St Andrews, Fife KY16 9SS, UK*

[11]*Aix Marseille Université, CNRS, LAM (Laboratoire d'Astrophysique de Marseille) UMR 7326, F-13388 Marseille, France*

[12]*Department of Physics and Astronomy, Macquarie University, NSW 2109, Australia*

[13]*Department of Physical Sciences, The Open University, Milton Keynes MK7 6AA, UK*

[14]*Max Planck Institut für Extraterrestrische Physik, Giessenbachstrasse 1, D-85748 Garching, Germany*

[15]*Institut d'Astrophysique et Géophysique, Université de Liège, allée du 6 Août 17, B-4000 Liège, Belgium*

[16]*Isaac Newton Group of Telescopes, Apartado de Correos 321, E-38700 Santa Cruz de Palma, Spain*

[17]*Department of Physics, University of Cambridge, J J Thomson Av, Cambridge CB3 0HE, UK*

[18]*Observatori Astronòmic de Mallorca, Camí de l'Observatori s/n 07144 Costitx, Mallorca, Spain*

[19]*Physics and Astronomy Department, Vanderbilt University, Nashville, TN 37235, USA*

[20]*Department of Physics, Fisk University, Nashville, TN 37208, USA*

This paper has been typeset from a TEX/LATEX file prepared by the author.